Title
Motion of nanovehicles on pristine and vacancy-defected silicene: implications for controlled surface motion

Authors
Youzi, Mehrdad
Kianezhad, Mohammad
Vaezi, Mehran
et al.

Publication Date
2023-10-19

DOI
10.1039/d3cp02835f

PCCP

ROYAL SOCIETY OF CHEMISTRY

PAPER

View Article Online
View Journal | View Issue

Cite this: *Phys. Chem. Chem. Phys.*, 2023, **25**, 28895

Motion of nanovehicles on pristine and vacancy-defected silicene: implications for controlled surface motion†

Mehrdad Youzi, [a] Mohammad Kianezhad, [b] Mehran Vaezi [c] and Hossein Nejat Pishkenari *[d]

Understanding the motion of surface-rolling nanomachines has attracted lots of attention in recent studies, due to their ability in carrying molecular payloads and nanomaterials on the surface. Controlling the surface motion of these nanovehicles is beneficial in the fabrication of nano-transportation systems. In the present study, molecular dynamics (MD) simulations alongside the potential energy analysis have been utilized to investigate the motion of C_{60} and C_{60}-based nanovehicles on the silicene monolayer. Nano-machine simulations are performed using molecular mechanic forcefield. Compared with graphene and hexagonal boron-nitride, the molecules experience a higher energy barrier on the silicene, which leads to a lower diffusion coefficient and higher activation energy of C_{60} and nanomachines. Overcoming the maximum energy barrier against sliding motion is more probable at higher temperatures where the nanomachines receive higher thermal energy. After evaluating the motion of molecules around local vacancies, we introduce a nanoroad structure that can restrict surface motion. The motion of C_{60} and nanovehicles over the surface is limited to the width of nanorods up to a certain temperature. To increase the controllability of the motion, a thermal gradient has been applied to the surface and the molecules move toward the lower temperature regions, where they find lower energy levels. Comparing the results of this study with other investigations regarding the surface motion of molecules on boron-nitride and graphene surfaces brings forth the idea of controlling the motion by silicene-based hybrid substrates, which can be further investigated.

Received 18th June 2023,
Accepted 6th October 2023

DOI: 10.1039/d3cp02835f

rsc.li/pccp

1. Introduction

Investigating the C_{60}-based nanocars and their motion on a variety of surfaces is a rapidly evolving field that has created significant interest due to their potential in the transportation of materials at the nanometer scale which has applications in different fields, including drug delivery,[1,2] nanoscale electronics,[3,4] and nanomaterials science.[5,6] Nanocars are molecular machines consisting of a chassis attached to axles and wheels made up of fullerene molecules.[7,8] The motion of these nanovehicles depends on their interaction with the surface on which they are placed.[9,10] Since these surface rolling molecules have demonstrated a great ability to transport molecular payloads across surfaces, numerous computational and experimental investigations have been prompted to achieve a controllable movement of these molecular machines.[11,12] Finding their way into many fields, optimization techniques are also showing promising results to better help scientists in the field of molecular simulations.[13–16]

Controllable surface motion has been achieved through the use of external agents, such as a temperature gradient[17,18] or an

[a] *Department of Civil and Environmental Engineering, University of California Irvine, Irvine, USA*
[b] *Department of Structural Engineering, University of California-San Diego, La Jolla, CA, 92093-0085, USA*
[c] *Institute for Nanoscience and Nanotechnology (INST), Sharif University of Technology, Tehran, Iran*
[d] *Mechanical Engineering Department, Sharif University of Technology, Tehran, Iran. E-mail: nejat@sharif.edu*

† Electronic supplementary information (ESI) available: Supplementary information of this study includes the employed parameters in the simulation of C_{60} and nanomachines. Force field parameters including the bonds, angles, dihedrals, and intermolecular interaction parameters for LJ potential are described in detail. Charge transfer between C_{60} and silicene monolayer has been analyzed using a first-principle calculation. We have also provided the RMS of velocity at various temperatures to be compared with the equipartition theorem for the validity of simulations. Velocity distribution is also studied to evaluate if there is a direction preference at various temperatures. Monovacancy migration is investigated to check the stability of the proposed nanoroad. The orientation of the nanocar with respect to the nanoroad is checked to prove the importance of how overcoming the barrier is correlated to the spatial configuration. The effect of the nanoroad on controlling the surface diffusivity of molecules is discussed at 100 to 700 K with 100 K intervals. Moreover, the effect of the proposed array of vacancies as the limiting agent for controlling the motion has also been surveyed by different placements of the nanocar with respect to the array. See DOI: **https://doi.org/10.1039/d3cp02835f**

electric field.[19] In this context, Lensen and Elemans[20] explored the use of scanning tunneling microscope (STM) to investigate and control the motion of molecular rotors on surfaces by performing tunneling current–time spectroscopy. Simpson *et al.*[21] focused on the use of STM to study and control the rotation of a single molecule. Shirai *et al.*[22] described the use of thermal energy to drive the motion of a nanocar along a surface and they debated about the design of nanocars and the mechanism by which the surface motions are steered in a particular direction. Computational methods have found their way in a variety of forms to help us explain the nature of processes.[23] Molecular simulations have also been extensively suggested to reach a comprehensive understanding of the surface motion behavior of nanomachines.[24,25] Nemati *et al.*[26] explored the effect of thermal gradients on the motion of molecules and proposed a method to steer their movement. The results suggest that non-uniform heat-induced substrates can be utilized to control the motion of molecules and achieve the targeted transportation on surfaces.

Furthermore, other techniques have been proposed to steer the motion of molecules over the substrate, which are based on surface modifications.[27,28] Vaezi *et al.*[29] studied the effect of strain gradient on the motion of C_{60} molecules and they demonstrated that the strain gradient of the surfaces leads to the directed motion of fullerene. Kianezhad *et al.*[29] investigated the unidirectional motion of C_{60}-based nanovehicles over a hybrid substrate of boron-nitride and graphene. It has been indicated that a hybrid substrate with a temperature gradient can be exploited to control the surface motion of nanocars. Hybrid substrates have also been probed by Nemati *et al.*[30] to control the diffusive motion of nanomachines. Due to the higher intermolecular attraction of nanocars and gold atoms, the surface motion of nanomachines is restricted to the gold region located in a silver substrate.

Surface motion on the monolayers is an area of interest in molecular dynamics, with implications for the development of advanced nanoscale devices and the understanding of various physical and chemical processes on these surfaces.[31,32] Considering the structural properties of these layers, such as graphene, boron nitride, and silicene, they can be considered a prime candidate for nanoscale mass transport.[33,34] Research studies mostly focused on the flat structures of graphene[35–37] and boron-nitride[38,39] as substrates for nano transportation purposes. The transport and diffusive motion of indium (In) adatoms across graphene after binding has been investigated recently, revealing a more growing interest in 2D surfaces.[40,41] These monolayers are able to form surface ripples leading to a wavy morphology affecting the surface motion.[42]

Being a two-dimensional material, silicene is composed of silicon atoms arranged in a honeycomb lattice similar to that of graphene.[43,44] The uncovering of the unique characteristics of graphene has sparked an increasing interest in its silicon and germanium counterparts (silicene and germanene).[45,46] The primary distinction between graphene and silicene or germanene is their inclination to create sp^2 hybridization for carbon and sp^3 and sp^2 for silicon and germanium.[47] This is evident in the fact that bulk Si/Ge has a diamond structure, while carbon is typically present in a graphitic form.[48] The unique electronic and mechanical properties of silicene, such as high carrier mobility and strong tensile strength, make it a promising candidate for a range of applications, including electronics and energy storage.[49–51] Hasan *et al.*[52] compared the surface wave on silicene to that of graphene, where they found that silicene has a higher surface wave velocity, which can be attributed to its higher stiffness and stronger interatomic bonding. As a result, evaluating the surface motion of the silicene is important as it is influenced by the mechanical and thermal properties of this two-dimensional material.

In this research, we investigated the surface motion of C_{60} and C_{60}-based nanomachines over a silicene monolayer by employing molecular dynamics simulations and potential energy analysis. Initially, the motion mechanism and dynamics of the molecules have been studied at various temperatures. To steer the motion and reach unidirectional movements, a nanoroad is designed on the surface which is based on the surface vacancies. The potential energy analysis and the characteristics of surface motion are obtained for nanomachines and fullerene at a variety of temperatures. The diffusivity of C_{60} is inspected in the presence and absence of the nanoroad to assess its effect. Aiming to achieve a more rectilinear motion, a temperature gradient is exerted on the surface. Further insight has also been provided by comparing the results with previous studies on the surface motion of C_{60} on graphene and boron-nitride.

2. Computational methods

Similar to the methodology used by Kianezhad *et al.*[53] to study the surface motion of CNTs over gold substrate, potential energy analysis and molecular dynamics simulations were employed to study the dynamics of nanovehicles on the silicene substrate. The surface dynamics of C_{60} (fullerene) and two C_{60}-based nanomachines which are named nanocar and nanotruck were inspected in this study. A schematic representation of C_{60}, nanocar, and nanotruck is depicted in Fig. 1, indicating the chemical formulation, molecular size, and atomic structure of molecules. C_{60} is a spherical symmetric molecule made of only carbon atoms and weighing 720.6 g mol^{-1}. It is known for being stable at high temperatures.[54,55] The chassis structure is the main difference between the C_{60}-based nanocar and nanotruck.[28] The C_{60}-based nanocar has a chassis made of carbon and hydrogen, which has a molecular mass of 3757.587 g mol^{-1}, with C_2 symmetry.[56] On the other hand, the C_{60}-based nanotruck has a more rigid chassis structure due to the addition of four nitrogen atoms along with carbon and hydrogen. The molecular mass of nanotruck is 3602.202 g mol^{-1} and has a D_2 symmetry, which gives it greater symmetry than the nanocar. Additionally, the nanotruck is smaller in size compared to the nanocar.[57]

Silicene is a two-dimensional monolayer material, and it possesses unique physical characteristics that have been extensively researched in recent years.[58–60] In 2010, the experimental

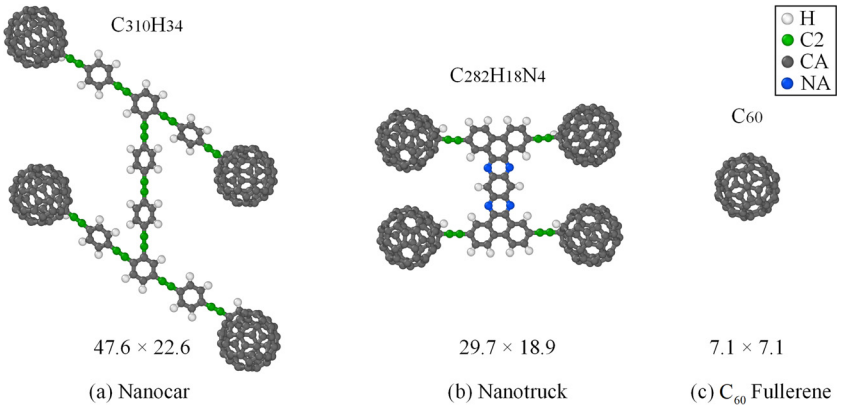

Fig. 1 Atomic structure of (a) C_{60}-based nanocar, (b) C_{60}-based nanotruck, and (c) C_{60} (fullerene). The molecular size and chemical formulation are indicated for each molecule.

formation of silicene was demonstrated on Ag(110)[48,61] and Ag(111)[62,63] substrates. Other surfaces, such as ZrB_2(0001),[64] Au(110),[65] and Ir(111)[66] have also been utilized to synthesize this two-dimensional material. Similar to graphene, the silicene monolayer here in this study has a hexagonal honeycomb configuration. However, unlike graphene, silicene is not flat, but has a periodically buckled topology,[67] which is a result of its sp^3 and sp^2 hybridization, because the silicon has a greater ionic radius compared to carbon.[58,60] In Fig. 2, the periodic structure of silicene and its buckled atomic arrangement is illustrated. The atomic structure of silicene can be defined by the lattice constant (a) and the buckling height (Δ). As presented in Fig. 2, the lattice constant of the silicene substrate in our simulations is 2.21 Å, and the buckling height is 0.8 Å.[68] It is worth mentioning that both the silicene monolayer and C_{60} and C_{60}-based nanovehicles are proven to be thermally stable in the temperature range of simulations of this investigation.[69–73]

In the current study, Tersoff potential[74] has been used to model the intramolecular interactions in the silicene monolayer, in which silicon point vacancies and their energetics show reasonable agreement with quantum mechanical results. Jannatul Islam *et al.*[75] have used this Tersoff potential for Si–Si interactions, to study the effects of different types of vacancies (bi-vacancy, point vacancy, mixed vacancy) and vacancy concentrations on the thermal conductivity of 2D silicon carbide. In another study, Rahman *et al.*[76] used Tersoff potential to study the thermal conductivity of pristine and defective silicene using molecular dynamics simulations. Moreover, Minh-Quy Le *et al.*[77] evaluated the effect of vacancies and Stone–Wales defects on the mechanical properties of silicene using Tersoff potential. In general, there are many studies evaluating the properties of pristine and defective silicene using Tersoff potential.[78–86] As it was reported by Mofidi *et al.*,[87] substrate ripples are considered in the simulations by this interatomic potential, which can change the dynamics of the surface rolling molecules due to the contact level variations. The intramolecular interactions of C_{60} is also modeled by the Tersoff potential.[88] To describe the internal interactions of the C_{60}-based nanomachines, the Molecular Mechanics (MM3) force field[89,90] was utilized. The bond and angle terms were modeled using a harmonic style, while the torsional terms were calculated using the dihedral style of the OPLS force field.[91,92] No improper terms were taken into account in the calculations. As presented in Fig. 1, two types of carbon atoms were considered with different hybridizations, labeled as "CA" and "C2", shown in black and green, respectively. The "CA" atoms in the simulations have either sp^2 or sp^3 hybridization, while the "CA" carbon atoms are sp^3[38] type. ESI† includes the parameters utilized in the simulations of C_{60} and C_{60}-based nanomachines.

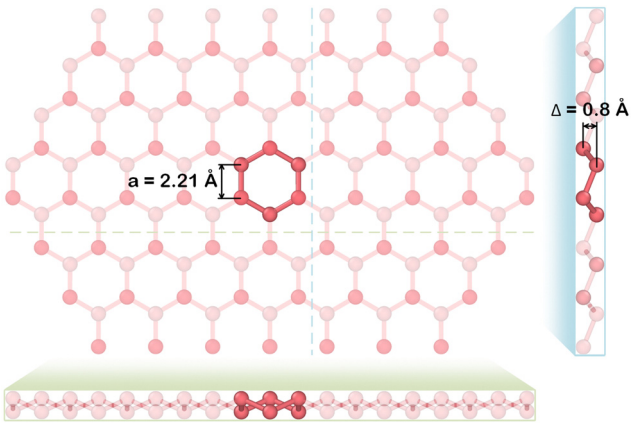

Fig. 2 A schematic view of the atomic structure of silicene, employed as the substrate in this investigation.[68]

In terms of intermolecular interactions between the molecules and the silicene substrate, to reduce the computational costs, the electrostatic forces were ignored. Akimov *et al.*[19] pointed out that in the absence of an external electric field, the charge transfer between non-bonded atoms is insignificant. To show this, a first principle calculation has been performed for a C_{60} over the silicene monolayer in the equilibrium distance to calculate the charge transfer. The charge transfer between the absorbed molecule and the surface was obtained by DFT calculations utilizing the Becke 3-parameter hybrid functional combined with the LeeYang–Parr correlation

functional (B3LYP),[93–95] with the basis set of 3-21G. The net charge transfer between the C_{60} and the silicene monolayer is 0.57 electrons. Ahangari *et al.*[96] calculated the net charge transfer from the nanocar to the gold substrate to be about 9.56 electrons. Nemati *et al.*[30] neglected this charge transfer in their calculations for proposing a hybrid silver/gold nanoroad. Moreover, while the charge transfer between C_{60} and gold is higher than silicene and C_{60},[97] electrostatic interactions are neglected in many studies.[9,27,28] A more detailed description of these calculations is provided in the ESI.†

Intermolecular interactions between the C_{60}/nanovehicles and the silicene substrate have been considered using the 6-12 Lennard-Jones (LJ) potential[98] with a cut-off radius of 13 Å. The ε and σ parameters used to model the non-bonding interactions between the molecules and the silicene substrate is presented in the ESI.† As indicated in the ESI,† the intermolecular interactions among the silicene surface and both carbon types in the nanomachines are modeled using identical non-bonding parameters, same as the C–Si interaction between fullerene atoms and silicene substrate.[38,99,100]

Simulations have been performed using Largescale Atomic/Molecular Massively Parallel Simulator[101] (LAMMPS) package and the integrations of equations of motion have been done by the velocity Verlet algorithm. To have a precise but not costly simulation, the time step has been set to 1 fs. Moreover, aiming to let the systems reach the equilibration before the simulation, they were relaxed at the desired temperatures for 200 ps. Inspired by our previous works,[29,102] to maintain a constant temperature, the Noose–Hover thermostat (*NVT* ensemble) is used, where the heat exchange rate between the system and the thermostat is determined by the temperature damping parameter (Tdamp), setting to 100 fs.

3. Results and discussion

The findings of our research are divided into four parts. In Section 3.1, we presented a detailed description of the motion of molecules on the silicene monolayer to establish a foundation for comprehending the substrate effect in contrast to earlier investigations.[29,36,38,103,104] In Section 3.2, we employ local vacancy defects to restrict the motion and examine the influence of vacancies on the movement parameters. In Section 3.3, we tried to manipulate and control the motion by applying a thermal gradient. Finally, in Section 3.4, we conduct a comparative analysis to gain a more profound understanding of the effect of substrates on the surface motions of molecules.

3.1 Free motion on silicene surface

The molecular dynamics method has been used to study the surface dynamics of C_{60} and C_{60}-based nanovehicles over a 140 Å × 140 Å silicene substrate. Simulations are conducted at 100 to 700 K with 100 K intervals for all three molecules (*i.e.*, C_{60} and two nanomachines). As described in the methodology section, simulations have been performed for 15 ns after a 200 ps of relaxation in the *NVT* ensemble. Trajectories of motion are depicted for C_{60} and C_{60}-based nanomachines in Fig. 3. The aforementioned trajectories are shown based on the center of mass (COM) of the molecules during the 15 ns simulation on the silicene monolayer.

Increasing the temperature intensifies the thermal fluctuations which in turn escalates the wavy structure of the 2D silicene monolayer, affecting the motion of surface molecules. As shown in Fig. 3, higher thermal energy increases the range of motion for C_{60}. While at 100 K the C_{60} range of motion is mostly limited to a couple of honeycombs, the molecule overcomes the

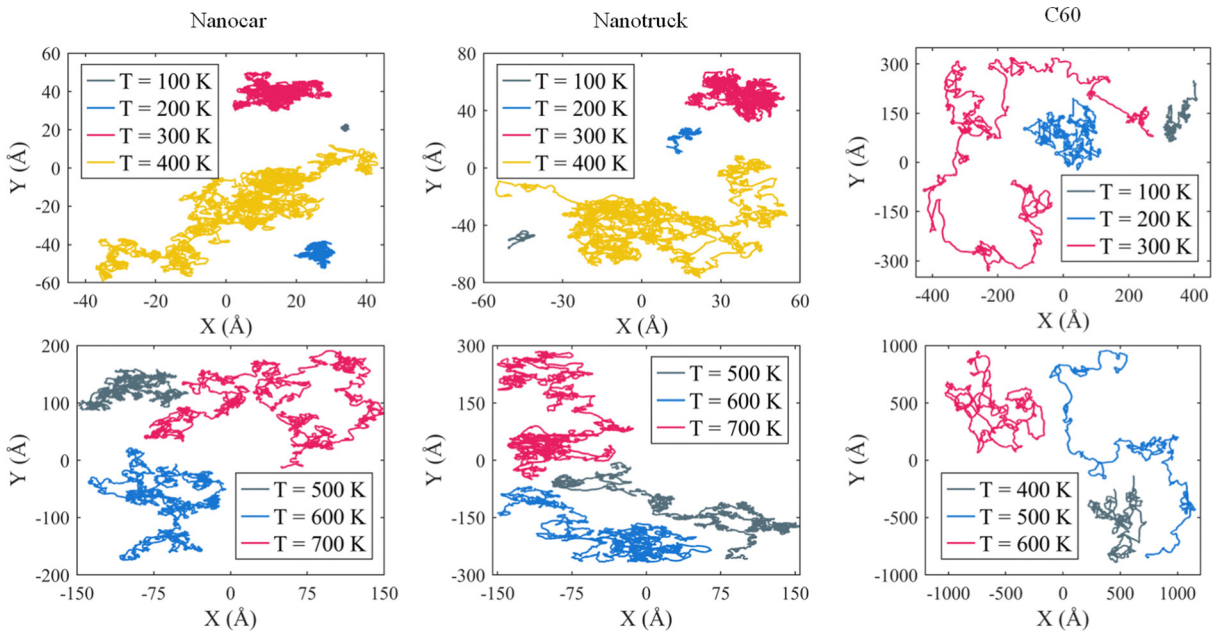

Fig. 3 Trajectories of motion for nanocar, nanotruck, and C_{60} at 100 to 700 K with 100 K intervals. Since desorption occurs for fullerene at 700 K, the C_{60} trajectory is not shown at the temperature of 700 K.

energy barrier against the transitional motions at higher temperatures. The same observation can be made for C_{60}-based nanocar and nanotruck. Higher intramolecular interactions between the nanomachines and the substrate decrease the range of motion compared to C_{60}.

It is worth mentioning that C_{60} was desorbed at 700 K from the silicene monolayer, meaning that the contribution of entropy in the Helmholtz free energy was so significant that the intermolecular interaction became negligible. Shortly after starting the simulation, the distance between the C_{60} and silicene became higher than the cut-off radius and they did not have any interactions afterward. To further evaluate the desorption temperature, we have simulated the C_{60} motion over the silicene at 25 K intervals between 600 and 700 K. The desorption did not happen during the 15 ns simulations at 675 K. As a result, considering a 25 K error bar, we can conclude that the desorption temperature for C_{60} is 675 $\pm$ 25 K, which is higher than the desorption temperature of fullerene on boron-nitride and graphene.[29,38,87,103]

Employing the mean square displacement (MSD) and diffusion coefficient, we aim to appraise the translational motion of fullerene. The MSD parameter is defined as:[105]

$$\mathrm{MSD}(t) = \langle |r(t) - r(0)|^2 \rangle \quad (1)$$

where, r is a position vector indicating the center of the mass (COM). The brackets are based on the notation used in statistical mechanics, representing ensemble averages over the phase space. In an ergodic system, this is equivalent to integrating the system over time.[106,107] The diffusion coefficient can be defined as the slop of the MSD as follows:[105]

$$D = \lim_{t\to\infty} \frac{1}{bt} \left\langle |r(t) - r(0)|^2 \right\rangle \quad (2)$$

Considering the fact that we are focusing on the surface dynamics over a 2D material, aiming to study the motion in the XY plane, b is considered to be equal to 4. It is worth mentioning that, to obtain a diffusion coefficient in three dimensions, b will be equal to 6.

To have a precise estimate of MSD, it is necessary to perform a large number of diverse simulations and then calculate the average based on the trajectory of all simulations. An alternative approach was established by Ernst and Kohler,[108] to carry out a longer simulation and divide the entire trajectory into several shorter trajectories. Since the first method is essentially costly, we divided the simulations into 30 smaller simulations with 500 ps duration and presented the MSD by averaging over these 30 sub-trajectories assuming that each interval is independent from the other since we are at the equilibrium.

MSD of the C_{60} and C_{60}-based nanomachines is depicted in Fig. 4 at different temperatures by calculating the sub-trajectory averages. For all three molecules, increasing the temperature results in higher MSD values showing a more diffusive motion over a larger area on the silicene monolayer. C_{60} has a weaker interaction with the monolayer due to a smaller number of particles, resulting in a higher diffusion coefficient and higher MSD compared to nanocar and nanotruck. Moreover, the MSD of the nanotruck is higher than nanocar which can be related to the structure of the chassis in the nanotruck. The nanotruck has a stiffer chassis that enables it to retain its motion direction on the silicene substrate. Conversely, the nanocar chassis is comparatively more flexible, which results in more frequent changes in its direction of motion. Similar observations have been made for boron-nitride and graphene substrate.[35,38,104]

Exploring the diffusion coefficient can be beneficial in comprehending the movement of molecules. MSD diagrams can be utilized to compute the diffusion coefficients. As depicted in Fig. 4, the slope of the MSD diagram for all molecules increases by escalating the temperature, pointing to a more diffusive motion which is in good match with the trajectories shown in Fig. 3. The diffusion coefficient for C_{60} is higher than the nanotruck at each temperature, and the nanotruck is higher than the nanocar. Further comparisons between this research and previous studies will be provided later in Section 3.4, which analyzes the effect of substrate on the diffusive motion.

In Fig. 5, $\ln(D)$ is presented as a function of $1/T$. Analyzing this diagram, known as Arrhenius plot, can provide insight on the mechanism of motion and activation energy. Using the Arrhenius analysis, we can find the potential energy barrier against the motion at low-temperature range, since the entropy share in Helmholtz free energy is negligible at lower temperatures. To describe the activation energy, we have used the Arrhenius equation.[109] This equation establishes the relation

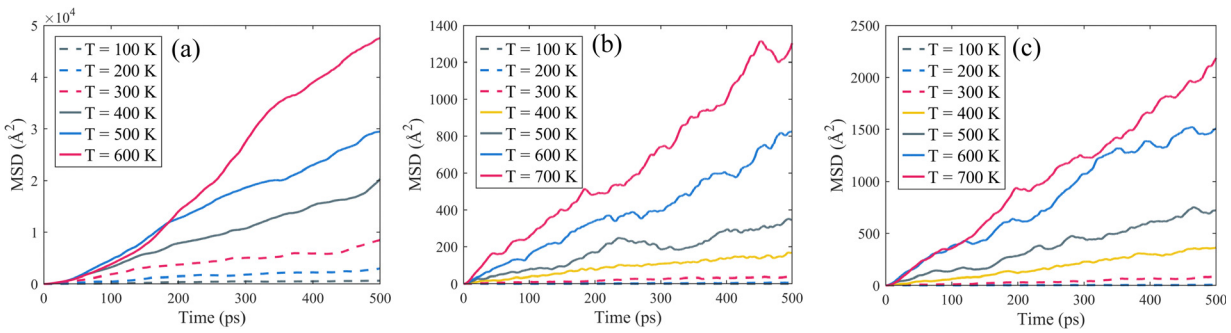

Fig. 4 Mean square displacement (MSD) of (a) C_{60}, (b) nanocar, and (c) nanotruck at 100 to 700 K with 100 K intervals as a function of time.

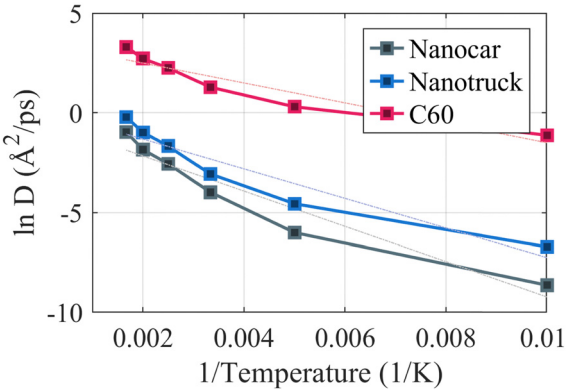

Fig. 5 Arrhenius analysis of the diffusion coefficient of C_{60} and C_{60}-based nanovehicles. Arrhenius analysis provides insight into the different regimes of motion.

between the activation energy of nanovehicles and their diffusion coefficient as follows:

$$D = D_0 \exp\left(-\frac{E_a}{k_B T}\right) \quad (3)$$

where k_B and T refer to the Boltzmann constant and temperature, respectively. The value of D_0, which represents the two-dimensional diffusion constant of nanomachines, is calculated using the Stokes–Einstein equation.[110]

Activation energy of the nanocar at 100 to 200 K range is 0.0453 eV while it is 0.0371 eV for nanotruck. As presented in Fig. 5, slope changes at 200 K for all three molecules, indicating the fact that the motion regime has changed at this temperature, and overcoming the energy barriers is easier as higher thermal energy is provided for nanomachines. The trajectory of motion and MSD of molecules are much smaller at 100 and 200 K compared to higher temperatures, approving the smaller slope of Arrhenius plot at lower temperatures. Raising the temperature, increases the contribution of entropy in Helmholtz free energy, resulting in a higher slope of the Arrhenius plot in Fig. 5. The activation energy at 200 to 700 K range is 0.1273 eV and 0.1105 eV for nanocar and nanotruck, respectively. The activation energy for the nanocar is higher than the nanotruck, pointing to the fact that higher energy is needed for nanocar to overcome energy barriers and move over the substrate. The larger activation energy of nanocar confirms its smaller diffusion coefficient compared to the nanotruck. This indicates that the nanotruck has a greater contribution of entropy in the Helmholtz free energy compared to the nanocar which is also in accordance with the MSD diagrams of Fig. 4 where the nanotruck exhibits greater mobility on the silicene surface.

Simulating the motion of C_{60} over the silicene monolayer indicates a smaller activation energy compared to the nanomachines. Activation energy of C_{60} at low and high temperatures (100 to 200 K and 200 to 700 K) is 0.0245 eV and 0.0758 eV, respectively, which is smaller than those of nanomachines. The C_{60} experiences a more diffusive motion due to a smaller number of atoms and lower intermolecular interactions with the substrate. Moreover, activation energy for C_{60} is considerably higher over the silicene monolayer compared to boron-nitride[38] and graphene[87] illuminating the higher interactions of the molecule with the silicene layer. It is worth noting that in order to verify the molecular dynamics results in this study, the RMS value of the transitional and angular velocities are obtained for C_{60} and are in agreement with the equipartition theorem (see Fig. S2 in ESI†). In addition, the distribution of the absolute velocity value for C_{60} at various temperatures is presented in Fig. S3, in the ESI,† with respect to the X-axis, showing the higher thermal energy of C_{60} as temperature increases.

A summary of the results obtained for motion over the silicene monolayer is provided in Table 1. Mean speed, as another parameter showing the ability of a molecule to move over a surface, is higher for C_{60} compared to nanomachines. Also, since the distribution of speed is mostly uniform, the mean velocity for all three molecules is almost zero. The vertical equilibrium distance calculated using the potential energy approach is 6.25 Å for C_{60} and 6.15 Å for nanomachines, while averaging the distance between the COM of molecules and the surface for C_{60} during the molecular dynamics simulations is 6.522 Å which is higher than the results of the potential energy analysis due to thermal fluctuations. On the other hand, this distance is lower than the potential energy analysis for nanomachines indicating higher intermolecular interactions. Moreover, the smaller vertical equilibrium distance for nanocar is due to the flexibility of the chassis compared to nanotruck. The anomaly parameter which is the slop of the $\log(D) - \log(t)$ diagram, is higher than 1 for C_{60} pointing to a super-diffusive

Table 1 A comparison of the surface motion of C_{60} and C_{60}-based nanomachines over the silicene monolayer

Parameters	C_{60}	Nanocar	Nanotruck
Molecular mass	720.6 g mol^{-1}	3757.587 g mol^{-1}	3602.202 g mol^{-1}
Dimension in X and Y direction	7.1 Å × 7.1 Å	47.6 Å × 22.6 Å	29.7 Å × 18.9 Å
Mean speed at 300 K	0.7415 Å ps^{-1}	0.3210 Å ps^{-1}	0.3387 Å ps^{-1}
Mean velocity at 300 K	0.0307 Å ps^{-1}	0.0008 Å ps^{-1}	0.0032 Å ps^{-1}
Vertical equilibrium distance (potential energy analysis)	6.25 Å	6.15 Å	6.15 Å
Vertical equilibrium distance at 300 K (molecular dynamics)	6.522 Å	5.655 Å	5.763 Å
Diffusion coefficient at 300 K	3.64 Å^2 ps^{-1}	0.0187 Å^2 ps^{-1}	0.047 Å^2 ps^{-1}
Anomaly parameter at 300 K	1.206	0.8541	0.7958
Activation energy at 300 K	75.8 meV	127.3 eV	110.5 eV
Regime of motion at 300 K	Super-diffusion	Sub-diffusion	Sub-diffusion

regime of motion, and is lower than 1 for nanovehicles revealing a sub-diffusive regime.[87]

3.2 Restricted motion around silicene vacancies

More efficient applications of nanomachines would be achieved by controlling the surface motion of nanovehicles.[28] The goal of this section is to limit the free motion of the C_{60} and nanomachines on the surface to have a more directional movement by modifying the substrate. We want to examine how effective is the energy barrier induced by surface vacancies, against the motion of nanovehicles and at which temperature range, the nanomachines have adequate thermal energy to deal with this barrier and move diffusively on the silicene substrate. In this section, the motion of nanomachines and C_{60} were simulated at the temperature range of 100 to 700 K with 100 K intervals. We have considered a series of local vacancies on the silicene substrate. Fig. 6 depicts the local vacancy effect on the intermolecular potential energy between the C_{60} and the silicene surface. It is worth noting that the energy required for making these vacancies is smaller than on graphene meaning that when subjected to intense laser irradiation with high-energy electrons and ions, the formation of structural defects in silicene would be significantly more likely to occur.[111] As a result, creating the nanoroad is plausible experimentally. It has also been mentioned that the monovacancy defects are easier to migrate in silicene compared to graphene.[111] A monovacancy migration analysis has been conducted on a silicene monolayer containing a vacancy to check the stability of the proposed nanoroad and the results are indicated in the ESI† in Fig. S4. It has been shown that the migration of the monovacancy happens at 700 K.

Hexagonal atomic configuration of the silicene monolayer is shown in the background of the intermolecular energy between C_{60} and the surface in Fig. 6 to better interpret the potential energy analysis. The potential energy between the molecule and surface has been obtained by moving the C_{60} incrementally over the 2D material horizontally. It is important to note that the vertical distance that corresponds to the lowest potential energy point in the Z direction is calculated using the line search algorithm, where at this equilibrium point, the minimum potential energy is determined and recorded. The vertical equilibrium distance of C_{60} over the silicene monolayer is 6.25 Å. Based on Fig. 6a, the C_{60} is more stable on the atoms with lower height, as it has lower potential energy there. The minimum potential energy that occurs on these atoms, is −0.8177 eV, and maximum potential energy that occurs on the upper atoms is −0.6370 eV. Potential energy analysis for local vacancy by removing one of the lower atoms of the buckled structure of the silicene substrate is presented in Fig. 6b. This local impurity creates a small energy barrier by increasing the potential energy over the neighboring upper atoms on the hexagonal structure of silicene. In this case, the maximum potential energy on the upper neighboring atoms increases to −0.5986 eV. On the other hand, it has been shown that by removing one of the atoms with higher height, while an energy well will be created on that spot, a higher energy barrier will also be formed around the potential energy well. This potential energy barrier and well which was induced by removing the top atoms (Fig. 6c), can be employed to restrict the motion in the horizontal directions. The minimum potential energy in this case is −0.9817 eV, which is happening for C_{60} on the position of the deleted upper atom. Also, the maximum potential energy in this situation is −0.5926 eV, occurring on the neighboring upper atoms, creating a higher energy barrier on the silicene. Consequently, we fabricated a nanoroad by removing a series of upper atoms to create an energy barrier and restrict the motion in molecular dynamics simulations.

Passing over the array of local vacancies, created by removing the upper atoms of the silicene monolayer, is also investigated for all three molecules using the potential energy analysis. Fig. 7a illustrates a schematic representation of the configuration considered for this assessment. Fig. 7b shows the potential energy variation as the nanomachines and C_{60} move over the array of local vacancies, obtained by the potential energy analysis. The shaded area for each diagram of Fig. 7b has been obtained by rotating each molecule by 1 degree

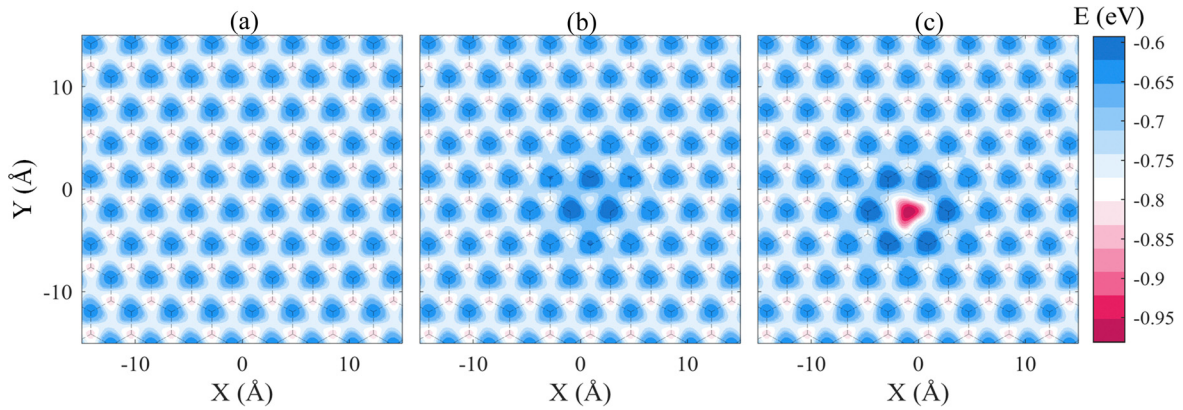

Fig. 6 Potential energy analysis calculated to reveal the surface dynamics of C_{60} and C_{60}-based nanomachines. (a) The intermolecular potential energy obtained by horizontally displacing C_{60} on the silicene substrate, (b) local vacancy effect on the intermolecular potential energy by removing one of the bottom atoms of the monolayer, and (c) effect of local vacancy on the intermolecular energy by removing one of the top atoms.

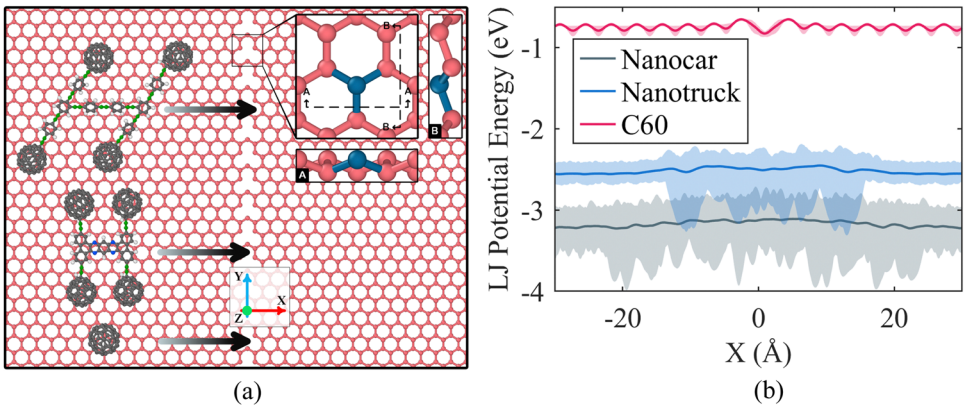

Fig. 7 (a) Schematic representation provided to depict the configuration utilized to assess the potential energy as the molecules traverse over the array of local vacancies. The coordinate system is shown in the figure for better interpretations, (b) the intermolecular LJ potential energy, is calculated using the potential energy analysis, when molecules are passing over the array of local vacancies. The array of defects is assumed to be at $X = 0$ for clarification purposes. The shaded area is the intermolecular interaction, obtained by rotating each molecule by 1-degree increments around their vertical axis. The darker lines are the average value of the shaded area for each molecule.

around the normal direction to the surface and finding the minimum potential energy by moving the molecule incrementally in the X direction by 0.5 Å steps. Considering the symmetrical structure of nanomachines, rotation of the molecules has been done by 90 degrees (*i.e.*, the range of [0.90]) around the normal axis to the XY plane. Passing C_{60} over the array of defects with different orientations does not highly affect the potential energy variation; however, overcoming the energy barrier for nanocar and nanotruck highly depends on how they approach the defect array and their spatial orientation around their Z axis. Intermolecular potential energy between the C_{60}-based nanocar and the silicene substrate is indicated for different angles in Fig. S5 in the ESI.† It can be deduced that the angle with which the nanocar encounters the array of vacancies is effective on the ability of the proposed nanoroad to steer the motion. In Fig. 7b, the average potential energy is presented as well, which shows the potential energy well and barrier when the C_{60} travels over the arrays of vacancies. As a result, this type of surface modification is more effective for controlling the motion of C_{60} due to its spherical shape and smaller size.

To better evaluate the effect of the proposed nanoroad, we have performed molecular dynamics simulations for 15 ns, and compared the results to the free motions. Fig. 8a illustrates the simulation setup for the surface motion of nanocar over the vacancy-based nanoroad. The width of the nanoroads in this section is correlated to the width of C_{60} and nanomachines. The road width for nanocar and nanotruck was considered to

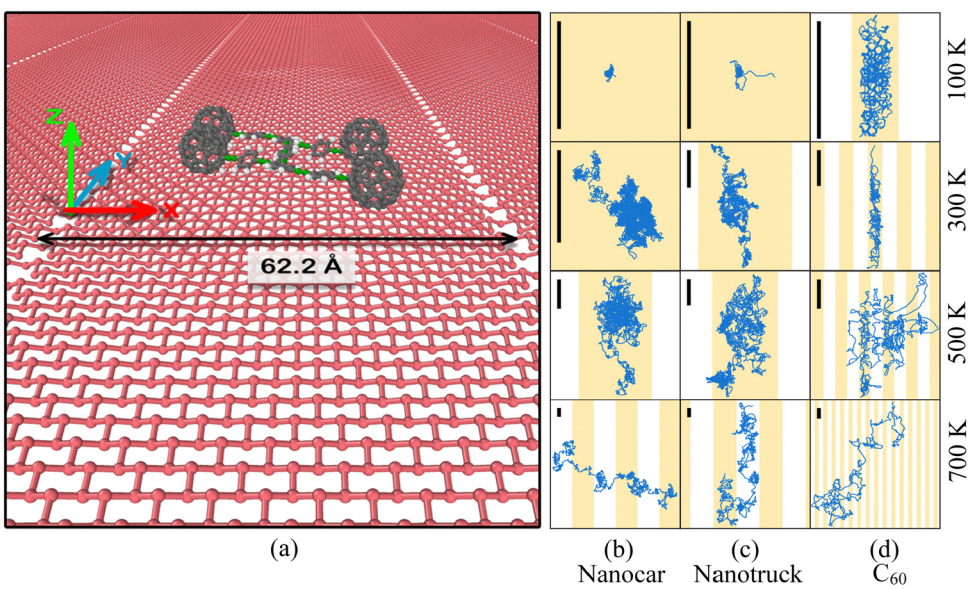

Fig. 8 (a) Graphical representation of the nanoroad created by the array of local vacancies. Trajectories of motion at 100, 300, 500, and 700 K for (b) nanocar, (c) nanotruck, and (d) C_{60}, showing the effect of nanoroad in restricting the motion on the silicene monolayer. Scale bar for C_{60} is 100 Å and for nanotruck and nanocar is 25 Å.

be 62.20 Å, and it was 39.58 Å for C_{60}. In other words, we considered three honeycombs on each side of the molecules, which gives the molecules sufficient space to move within the road. Also, the box dimension in the *X* direction has changed in a way that the width of the neighboring roads, created by periodic boundary conditions on the left and right sides, will be identical to the one in the middle. Simulations have been conducted at 100 to 700 K with 100 K intervals to further evaluate the temperature efficacy on the limited movement of C_{60} and nanomachines.

Fig. 8b–d show the trajectories of the motion for C_{60}-based nanocar, nanotruck, and fullerene, respectively. For the sake of simplification, only 100, 300, 500, and 700 K results are presented here. Trajectories of motion for all three molecules at all 7 temperatures are indicated in the Fig. S6 of ESI.† The surface motion of C_{60} is fully limited to the nanoroad during the simulation up to 300 K, showing the effect of the energy barrier. At 400 K, sufficient thermal energy is supplied for the C_{60} to overcome the energy barrier occasionally (Fig. S6, ESI†). At higher temperatures, C_{60} is able to overcome the energy barrier frequently; however, the diffusivity is decreased for motion over the nanoroad compared to free motion, which will be discussed later on. Studying the trajectory of motion for nanotruck reveals that the motion is limited to the nanoroad up to 400 K, while in the case of nanocar, overcoming the barrier first happens at 600 K (Fig. S6, ESI†). This is in accordance with the fact that chassis rigidity has made nanotruck more capable of preserving its motion direction, so overcoming the barrier occurs at lower temperatures, while nanocar will be driven away when one of its wheels encounters the barrier due to its flexibility. In other words, the flexibility of the chassis of nanocar wastes some part of the molecules energy, and the nanocar requires more thermal energy to escape the nanoroad. As a result, compared to nanotruck, nanocar will remain in the nanoroad up to the higher temperature of 600 K. Moreover, to have a more in-depth knowledge of the effect of the array of vacancies on the surface motion of nanovehicles, a group of simulations is conducted on controlling the surface motion of the nanocar at 100, 300, and 500 K by placing an array of vacancy exactly under the chassis, placing two arrays in a way that the wheels are on the outer side of the proposed nanoroad, and initially placing two wheels on the potential well created by the nanoroad to better interpret the effect of nanoroad. Results are indicated in Fig. S7, in the ESI.†

To further analyze the effect of the nanoroad on restricting the motion over the silicene monolayer, we have compared the diffusion coefficient for C_{60} and nanomachines at different temperatures. Fig. 9 presents the diffusion coefficient in the presence of the nanoroad and in the case of a surface free motion for all three molecules at various temperatures. Results indicate that the proposed nanoroad has decreased the diffusion coefficients of the motion in all cases. It should be mentioned that while in free surface motion, desorption had happened at 700 K for C_{60}, it did not occur in the presence of nanoroad during the simulation. As demonstrated before, for the surface free motion, the diffusion coefficient is higher for

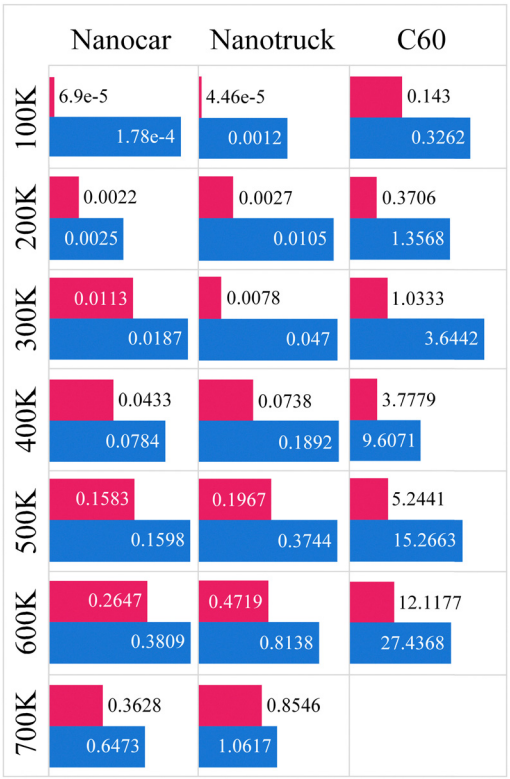

Fig. 9 Diffusion coefficient of C_{60} and C_{60}-based nanomachines at various temperatures in the presence (red) and absence (blue) of the nanoroad. C_{60} has been desorbed during the 15 ns simulation at 700 K in surface free motion.

C_{60} than nanomachines, and for nanotruck is higher than the nanocar. Nevertheless, this result is different in the presence of the nanoroad. For the nanotruck, the diffusion coefficient is significantly higher than the nanocar at higher temperatures while at lower temperatures (lower than 400 K), the diffusion coefficient of nanotruck is almost equal to or is slightly smaller than the nanocar. This has happened because of the rigidity of the chassis in the nanotruck, where at low temperatures, since nanotruck still does not have ample energy to easily overcome the barrier when it encounters the energy barrier the whole molecule needs to rotate decreasing the diffusion coefficient. On the other hand, nanocar is more flexible and when a wheel encounters the barrier at low temperatures it can easily move away.

3.3 Thermal gradient on vacancy-based nanoroads

To further steer the surface motion and control the diffusivity of the motion of molecules on the silicene monolayer, the effect of thermal gradient has been surveyed in this section. To apply the thermal gradient on the silicene substrate, the following process is implemented. A silicene monolayer of 500 Å length with the same width as the previous section is considered for each molecule, as presented in Fig. 8a. To prevent large movements, two regions of fixed atoms with a spacing of 10 Å are considered by setting the force components applied to them to zero. Five equally spaced intervals of 10 Å are considered to

create a thermal gradient from 600 to 300 K by applying *NVT* ensembles. Finally, *NVE* ensembles are exerted on the remainder of atoms between the *NVT* groups. To create the desired thermal gradient, the system has been relaxed for 1 ns before starting the simulation. To go through the effect of thermal gradient on directing the motion and how a combination of thermal gradient and the proposed nanoroad is effective, C_{60} is placed at the lower end of the substrate, where the temperature is 600 K. The simulation continues until the center of mass of the molecule reaches the upper side of the surface, where the temperature is 300 K, and the simulation stops using the halt command in LAMMPS.[101] Naturally, C_{60} moves toward the lower temperature regions, seeking lower energy.

The initial velocity can affect the trajectory of the motion of the molecule; especially, in this case, where overcoming the barrier can be also related to the orientation of the molecule in which it encounters the energy barrier. As a result, we have performed 20 different simulations for both cases (*i.e.*, with and without the nanoroad) and the resultant trajectories are shown in Fig. 10. The red shade is the area covered by the C_{60} motion during 20 simulations in the presence of nanoroad (two arrays of local vacancies), and the blue shade is the region covered by the motion of C_{60} in the absence of nanoroad, where there is no surface modification. It can be seen that the combination of the nanoroad and thermal gradient is more effective in controlling the surface motion of C_{60}, as expected. In the presence of the nanoroad the covered area by C_{60} over the substrate has decreased significantly. Due to the thermal gradient of the substrate, the fullerene finds directed motion along the direction of the *Y*-axis. The molecule moves from higher thermal energy (warmer region at 600 K) to the colder region of the substrates (300 K).

The trajectory of motion for one of the simulations in the equal initial conditions over the pristine and vacancy-defected silicene in Fig. 11 shows how effective the nanoroad is in controlling the surface motion of C_{60} in the presence of the thermal gradient. It is evident that in the absence of the

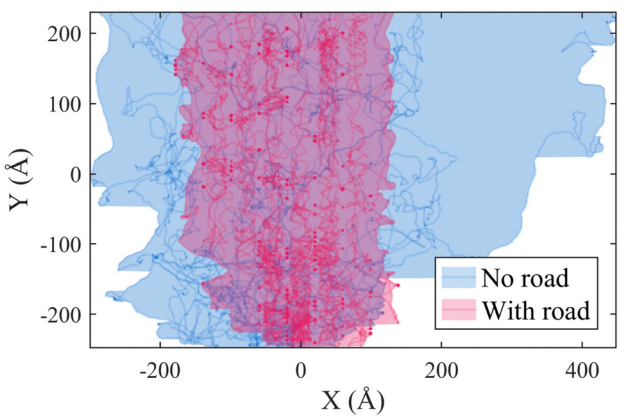

Fig. 10 Evaluating the effect of thermal gradient on the motion of C_{60} in the presence (red) and absence (blue) of the nanoroad. The shaded area is the regions that were covered by the motion of C_{60}, as a result of 20 different molecular simulations.

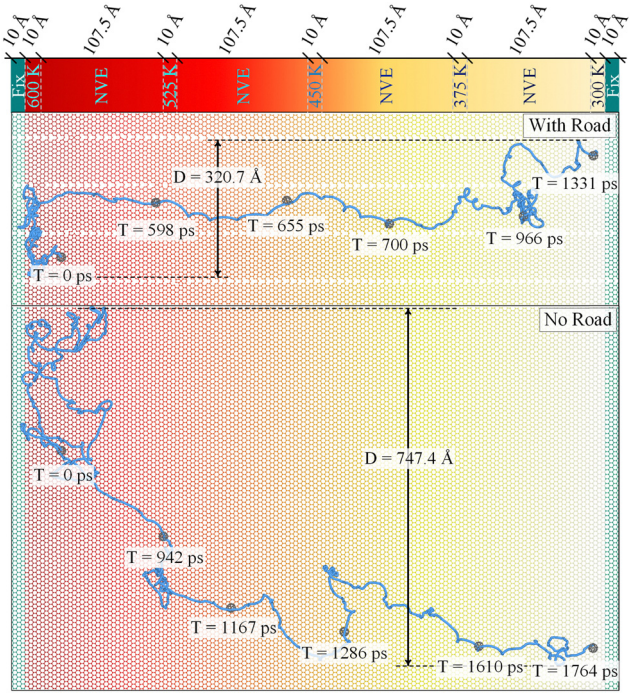

Fig. 11 Manifestation of the effect of nanoroad on controlling the motion of C_{60} when the temperature gradient is applied to the silicene substrate by showing the trajectory of motion of one of the simulations. By applying the temperature gradient, the motion of the C_{60} in the presence of the nanoroad is limited, while over the pristine silicene monolayer, C_{60} experiences more transversal motion. Applied thermal gradient using molecular ensembles of *NVT* and *NVE* to the substrate is indicated on top.

nanoroad, C_{60} has more transverse movements compared to the case where the nanoroad is present. It is worth mentioning that at high temperatures, the vacancy often disappears by atomic rearrangements. This behavior can be spotted in some regions (mostly at the higher temperature end due to provided higher thermal energy) in Fig. 11 when the thermal gradient is applied to the nanoroad. The elapsed time in each case is indicated in Fig. 11, showing that the C_{60} can reach the other end of the substrate faster when the nanoroad is there. Also, the configuration of *NVT* and *NVE* ensembles are presented in Fig. 11 with their spacing.

Fig. 12 demonstrates the motion of two nanomachines on the temperature-gradient substrates in the presence and absence of nanoroad structure. According to this figure, the employed nanoroad had no significant effect on the displacement range of nanomachines in the direction of *X*-axis. However, due to the temperature gradient of the substrate, the nanomachines show directional motion along the *Y*-axis. To constrain the motion of nanovehicles in the *X*-axis direction, narrower nanoroads are required. By dividing the simulations into equal intervals (500 ps independent simulations), the diffusion coefficient is calculated to better clarify the effect of nanoroad on restricting the motion. The average of the diffusion coefficient of the conducted 20 simulations for the surface motion of C_{60} in the presence of the nanoroad, when the thermal gradient is applied is 8.26 $Å^2\ ps^{-1}$, while in the absence

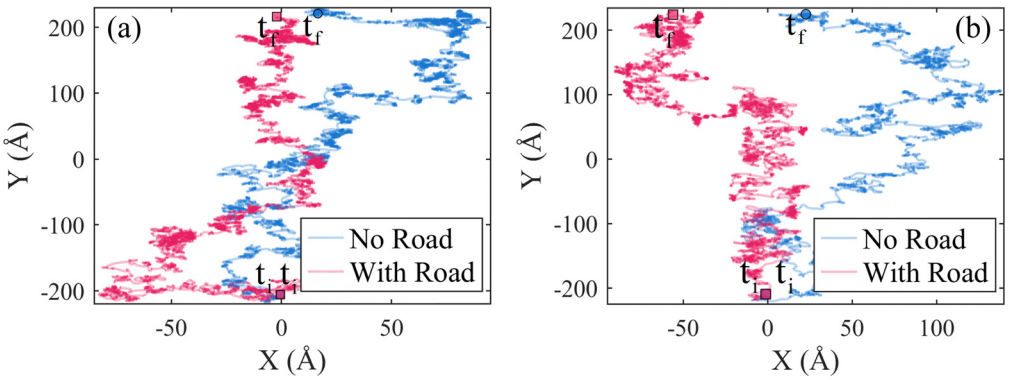

Fig. 12 Thermal gradient effect on the motion over the silicene substrate for (a) nanocar and (b) nanotruck in the presence (red) and absence (blue) of the nanoroad. Results indicate a small restriction of the motion in these cases.

of the nanoroad it is 21.11 $Å^2$ ps^{-1}, revealing the effect of the nanoroad on limiting the diffusion of C_{60}. However, studying the average diffusion coefficient for nanotruck and nanocar indicates insignificant changes. Diffusion coefficient for the nanotruck in the absence of the nanoroad, when only the thermal gradient is applied, is 0.32 $Å^2$ ps^{-1} and for the combined effect of thermal gradient and nanoroad is 0.14 $Å^2$ ps^{-1}. For nanocar on the other hand, whether in the presence of the nanoroad or when only a thermal gradient is exerted, the diffusion coefficient is about 0.11 $Å^2$ ps^{-1}. The limitation effect of the nanoroad on controlling the diffusivity of motion of the nanotruck is due to the rigidity of the chassis, decreasing the diffusivity when the molecule encounters the energy barrier. Conversely, the flexibility of the chassis of nanocar helps the molecule to continue the motion as it encounters the energy barriers created by local vacancies.

3.4 Comparing the surface motion on silicene, graphene, and hexagonal boron-nitride

In this section, we compare the results obtained in this study with previous investigations on the surface dynamics of other 2D materials. By comparing the motion over various surfaces, we can enhance our ability to select the suitable 2D material for controlling the motion.[39] Many studies have been conducted in recent years on the effect of substrate,[9,87,112] surface manipulations,[21,27,28] and combining surfaces[29,30] to steer the surface dynamics of molecules. Graphene[32,104,113] and boron-nitride[38,39] are mostly researched 2D materials for surface motion and similarity in structure and mechanical properties[43] brings forth the idea of an analogy of surface motion. Table 2 provides a comprehensive comparison between the properties of motion over graphene, hexagonal boron-nitride, and silicene for C_{60}. As presented in Table 2, there are some differences between the surface motion characteristics of silicene and the other two monolayers.

Due to higher attraction between C_{60} and silicene, the vertical equilibrium distance is lower compared to boron-nitride and graphene. This higher intermolecular interaction has also caused a significantly smaller diffusion coefficient at various temperatures. The diffusion coefficient of fullerene over the silicene monolayer at room temperature is 3.64 $Å^2$ ps^{-1} which is noticeably smaller than 31.00 $Å^2$ ps^{-1} and 70.00 $Å^2$ ps^{-1}, the diffusion coefficient for surface free motion of C_{60} over boron-nitride and graphene, respectively. As a result, the anomaly parameter (power-law dependence on time) is smaller over the silicene compared to the other 2D materials at the same temperature. According to Fig. 6, the maximum energy barrier against sliding (*i.e.*, the energy required to move freely over the surface), which is the difference between the highest and the lowest energy, is 180.6 meV over the silicene. The minimum energy barrier against sliding, which is the energy needed to move over the atoms with lower height, is 65.3 meV. The C_{60} does not have the required energy to move freely over the surface at low temperatures, so the motion is mostly restricted to the movements of the atoms with lower height in the buckled structure of silicene, where the molecule requires lower thermal energy. The higher potential energy on the upper atoms (presented in Fig. 2) limits the motion at low

Table 2 Comparing the surface motion of C_{60} over silicene, hexagonal boron-nitride, and graphene[29,35,38,39,87,115]

Parameters	Silicene	Boron-nitride	Graphene
Vertical equilibrium distance	6.25 Å	6.4 Å	6.4 Å
Thermal energy required for desorption	818 meV	940 meV	650 meV
Desorption temperature	675 ± 25	650 ± 25	550 ± 25
Maximum energy barrier against sliding	180.6 meV	12.7 meV	14.1 meV
Minimum energy barrier against sliding	65.3 meV	2.5 meV	1.4 meV
Diffusion coefficient at 300 K	3.64 $Å^2$ ps^{-1}	31.00 $Å^2$ ps^{-1}	70.00 $Å^2$ ps^{-1}
Anomaly parameter at 300 K	1.206	1.52	1.71
Activation energy at 300 K	75.8 meV	89.0 meV	39.2 meV
Regime of motion at 300 K	Super-diffusion	Super-diffusion	Super-diffusion

temperatures. However, by increasing the temperature overcoming the maximum energy barrier against sliding will be more frequent. These two values for graphene and boron-nitride are considerably smaller than silicene. We can conclude that in a hybrid substrate, nanomachines are more attracted to silicene. This notion brings forth the idea of the fabrication of nanoroad composed of silicene and other 2D materials to steer the surface dynamics of the nanovehicles. Also, carbon structures, including C_{60} and nanovehicles are hydrophobic,[114] meaning that if we have a surface of hydrophilic material, molecules are better capable of overcoming the barrier and better move, especially in this study where the intermolecular interactions with silicene are higher than other 2D substrates. As a suggestion, we can cover the surface of silicene with oxygen atoms, and since the ε in the LJ for oxygen–carbon is much smaller than for silicon–carbon, molecules will be more capable of moving over the surface. This idea can solve the smaller mobility problem over the silicene substrate.

The insight provided by comparing the thermal energy needed for desorption indicates that the C_{60} requires 818 meV to be desorbed. The desired desorption thermal energy is in fact the global minimum of the potential energy between the fullerene and the silicene monolayer. This value is 940 meV for boron-nitride and 650 meV for graphene. This outcome points out that the desorption of the C_{60} over the silicene is comparable to boron-nitride and it should be higher than graphene. Molecular simulations indicate that the desorption of C_{60} has happened at 700 K during our 15 ns simulation, while it did not occur at 675 K. Consequently, the desorption temperature over the silicene is 675 $\pm$ 25 K while for boron-nitride[38] and graphene[87] it was 650 $\pm$ 25 K and 550 $\pm$ 25 K, respectively.

4. Conclusion

Based on its potential applications in electronics and nanotechnology, silicene has garnered significant interest in recent years. In this study, the surface dynamics of C_{60} and two C_{60}-based nanomachines (nanocar and nanotruck) are investigated using molecular dynamics simulations and potential energy analysis. Surface free motion of nanomachines has indicated that the diffusion coefficient is smaller on silicene compared to boron-nitride and graphene monolayers, due to the higher energy barriers on silicene monolayer, resulting in higher activation energy. Higher thermal energy is needed for desorption alongside the fact that the desorption temperature is higher for silicene compared to graphene brings forth the idea of controlling the surface motion by fabrication of a hybrid substrate. Nevertheless, this idea requires further analysis.

At low temperatures, the motion is mostly restricted to the movements of the atoms with lower height, since enough energy is not yet provided to overcome the maximum energy barrier against free translations. However, by increasing the temperature, entropy share in the Helmholtz free energy increases, and overcoming the barriers is more frequent. It has been shown that the diffusivity of the motion of C_{60} is more than nanomachines, due to its lower intermolecular interactions. Moreover, it has been indicated that the diffusivity of the motion of nanotruck is higher than nanocar, pointing to the smaller activation energy of nanotruck as a result of its rigid chassis and the ability to preserve the motion direction.

Based on the potential energy analysis, an array of local vacancies has been designed (named nanoroad structure) to limit the motion of C_{60} and nanomachines. It has been displayed that in all cases the displacement range has been decreased and limited. Nonetheless, the spatial orientation with which the nanomachines encounter the vacancy is effective in overcoming the energy barrier. For the surface free motion, the diffusion coefficient for the nanotruck is always higher than nanocar. However, in the presence of the proposed nanoroad, the rigid chassis of the nanotruck decreases the diffusion coefficient at low temperatures. On the other hand, the flexible chassis of nanocar help the nanomachines to better move inside the vacancy-based nanoroads. To further analyze the motion controllability, a temperature gradient has been applied to the substrate and the effect of the nanoroad has been studied in the presence of temperature gradient. It has been revealed that the displacement ranges of motion and the area that C_{60} covers during the motion on the silicene monolayer have decreased significantly when we applied the temperature gradient on the nanoroad. Additionally, the trajectories of the motion of C_{60} and nanomachines revealed that the molecules experience a directed motion from the areas with high-temperature to the low-temperature regions.

Author contributions

Mehrdad Youzi: performing simulations, writing and editing the manuscript, data analysis, and preparing figures. Mohammad Kianezhad: performing simulations, data analysis, and figure preparation. Mehran Vaezi: editing the manuscript, analyzing the data, and providing discussions. Hossein Nejat Pishkenari: supervision, proposing the idea of the project, editing the manuscript, and providing discussions.

Data availability

The computational protocols used in this work, the input and output files, are available upon request.

Conflicts of interest

The authors declare no competing interests.

References

1 Y. Yao, Y. Zhou, L. Liu, Y. Xu, Q. Chen and Y. Wang, *et al.*, Nanoparticle-Based Drug Delivery in Cancer Therapy and Its Role in Overcoming Drug Resistance, *Front. Mol. Biosci.*, 2020, 7, 193.

2 W. Gao and J. Wang, Synthetic micro/nanomotors in drug delivery, *Nanoscale*, 2014, **6**(18), 10486–10494.
3 T. Kudernac, N. Ruangsupapichat, M. Parschau, B. Maciá, N. Katsonis and S. R. Harutyunyan, *et al.*, Electrically driven directional motion of a four-wheeled molecule on a metal surface, *Nature*, 2011, **479**(7372), 208–211.
4 L. H. Madkour, *Nanoelectronic Materials: Fundamentals and Applications*, Springer International Publishing, 2019, Advanced Structured Materials.
5 D. A. Leigh, J. K. Y. Wong, F. Dehez and F. Zerbetto, Unidirectional rotation in a mechanically interlocked molecular rotor, *Nature*, 2003, **424**(6945), 174–179.
6 T. Jin, V. García-López, S. Kuwahara, P.-T. Chiang, J. M. Tour and G. Wang, Diffusion of Nanocars on an Air–Glass Interface, *J. Phys. Chem. C*, 2018, **122**(33), 19025–19036.
7 G. Vives and J. M. Tour, Synthesis of Single-Molecule nanocars, *Acc. Chem. Res.*, 2009, **42**(3), 473–487.
8 K. Ariga, T. Mori and W. Nakanishi, Nano Trek Beyond: Driving Nanocars/Molecular Machines at Interfaces, *Chem. – Asian J.*, 2018, **13**(10), 1266–1278.
9 H. Nejat Pishkenari, A. Nemati, A. Meghdari and S. Sohrabpour, A close look at the motion of C60 on gold, *Curr. Appl. Phys.*, 2015, **15**(11), 1402–1411.
10 A. Akimov and A. B. Kolomeisky, Dynamics of Single-Molecule Rotations on Surfaces that Depend on Symmetry, Interactions, and Molecular Sizes, *J. Phys. Chem. C*, 2011, **115**(1), 125–131.
11 R. Li, B. An, J. Liu and Q. Peng, Modulating Directional Movement of Graphene Nanoflake Using a Channel, *Crystals*, 2022, **12**(12), 1830.
12 S. M. Hosseini Lavasani, H. Nejat Pishkenari and A. Meghdari, How Chassis Structure and Substrate Crystalline Direction Affect the Mobility of Thermally Driven p-Carborane-Wheeled Nanocars, *J. Phys. Chem. C*, 2019, **123**(8), 4805–4824.
13 A. R. Khoei and M. Kianezhad, A machine learning-based atomistic-continuum multiscale technique for modeling the mechanical behavior of Ni3Al, *Int. J. Mech. Sci.*, 2023, **239**, 107858.
14 S. Salehi, I. Miremadi, M. Ghasempour Nejati and H. Ghafouri, Fostering the Adoption and Use of Super App Technology, *IEEE Trans. Eng. Manag.*, 2023, 1–15.
15 S. Habib, S. Aghakhani, M. G. Nejati, M. Azimian, Y. Jia and E. M. Ahmed, Energy management of an intelligent parking lot equipped with hydrogen storage systems and renewable energy sources using the stochastic p-robust optimization approach, *Energy*, 2023, **278**, 127844.
16 H. Kosarirad, M. G. Nejati, A. Saffari, M. Khishe and M. Mohammadi, Feature Selection and Training Multilayer Perceptron Neural Networks Using Grasshopper Optimization Algorithm for Design Optimal Classifier of Big Data Sonar, *J. Sensors*, 2022, 1–14.
17 L. Grill, K.-H. Rieder, F. Moresco, G. Rapenne, S. Stojkovic and X. Bouju, *et al.*, Rolling a single molecular wheel at the atomic scale, *Nat. Nanotechnol.*, 2007, **2**(2), 95–98.
18 M. Becton and X. Wang, Thermal Gradients on Graphene to Drive Nanoflake Motion, *J. Chem. Theory Comput.*, 2014, **10**(2), 722–730.
19 A. V. Akimov and A. B. Kolomeisky, Unidirectional Rolling Motion of Nanocars Induced by Electric Field, *J. Phys. Chem. C*, 2012, **116**(42), 22595–22601.
20 D. Lensen and J. A. A. W. Elemans, Artificial molecular rotors and motors on surfaces: STM reveals and triggers, *Soft Matter*, 2012, **8**(35), 9053–9063.
21 G. J. Simpson, V. García-López, A. Daniel Boese, J. M. Tour and L. Grill, How to control single-molecule rotation, *Nat. Commun.*, 2019, **10**(1), 4631.
22 Y. Shirai, A. J. Osgood, Y. Zhao, K. F. Kelly and J. M. Tour, Directional Control in Thermally Driven Single-Molecule Nanocars, *Nano Lett.*, 2005, **5**(11), 2330–2334.
23 A. R. Khoei, S. Saeedmonir, N. Hosseini and S. M. Mousavi, An X–FEM technique for numerical simulation of variable-density flow in fractured porous media, *MethodsX*, 2023, **10**, 102137.
24 A. V. Akimov, A. V. Nemukhin, A. A. Moskovsky, A. B. Kolomeisky and J. M. Tour, Molecular dynamics of surface-moving thermally driven nanocars, *J. Chem. Theory Comput.*, 2008, **4**(4), 652–656.
25 A. Lohrasebi, M. Neek-Amal and M. R. Ejtehadi, Directed motion of C60 on a graphene sheet subjected to a temperature gradient, *Phys. Rev. E: Stat., Nonlinear, Soft Matter Phys.*, 2011, **83**(4 Pt 1), 42601.
26 A. Nemati, H. Nejat Pishkenari, A. Meghdari and S. S. Ge, Directional control of surface rolling molecules exploiting non-uniform heat-induced substrates, *Phys. Chem. Chem. Phys.*, 2020, **22**(46), 26887–26900.
27 A. Nemati, H. Nejat Pishkenari, A. Meghdari and S. S. Ge, Influence of Vacancies and Grain Boundaries on the Diffusive Motion of Surface Rolling Molecules, *J. Phys. Chem. C*, 2020, **124**(30), 16629–16643.
28 A. Nemati, H. Nejat Pishkenari, A. Meghdari and S. Sohrabpour, Directing the diffusive motion of fullerene-based nanocars using nonplanar gold surfaces, *Phys. Chem. Chem. Phys.*, 2018, **20**(1), 332–344.
29 M. Kianezhad, M. Youzi, M. Vaezi and H. Nejat Pishkenari, Unidirectional motion of C60-based nanovehicles using hybrid substrates with temperature gradient, *Sci. Rep.*, 2023, **13**(1), 1100.
30 A. Nemati, H. Nejat Pishkenari, A. Meghdari and S. S. Ge, Controlling the Diffusive Motion of Fullerene-Wheeled Nanocars Utilizing a Hybrid Substrate, *J. Phys. Chem. C*, 2019, **123**(42), 26018–26030.
31 W. Bao, F. Miao, Z. Chen, H. Zhang, W. Jang and C. Dames, *et al.*, Controlled ripple texturing of suspended graphene and ultrathin graphite membranes, *Nat. Nanotechnol.*, 2009, **4**(9), 562–566.
32 M. Vaezi, H. Nejat Pishkenari and M. R. Ejtehadi, Collective movement and thermal stability of fullerene clusters on the graphene layer, *Phys. Chem. Chem. Phys.*, 2022, **24**(19), 11770–11781.
33 Y. Li, X. Liu, C. Chen, J. Duchamp, R. Huang and T.-F. Chung, *et al.*, Differences in self-assembly of spherical C60 and planar PTCDA on rippled graphene surfaces, *Carbon N Y*, 2019, **145**, 549–555.

34 I. Leven, I. Azuri, L. Kronik and O. Hod, Inter-layer potential for hexagonal boron nitride, *J. Chem. Phys.*, 2014, **140**(10), 104106.
35 S. M. Mofidi, H. Nejat Pishkenari, M. R. Ejtehadi and A. V. Akimov, Locomotion of the C60-based nanomachines on graphene surfaces, *Sci. Rep.*, 2021, **11**(1), 2576.
36 M. Neek-Amal, N. Abedpour, S. N. Rasuli, A. Naji and M. R. Ejtehadi, Diffusive motion of C60 on a graphene sheet, *Phys. Rev. E: Stat., Nonlinear, Soft Matter Phys.*, 2010, **82**(5 Pt 1), 51605.
37 C. Lundgren, A. Kakanakova-Georgieva and G. K. Gueorguiev, A perspective on thermal stability and mechanical properties of 2D Indium Bismide from ab initio molecular dynamics, *Nanotechnology*, 2022, **33**(33), 335706.
38 M. Vaezi, H. Nejat Pishkenari and A. Nemati, Mechanism of the motion of nanovehicles on hexagonal boron-nitride: A molecular dynamics study, *Comput. Mater. Sci.*, 2022, **207**, 111317.
39 M. Vaezi, H. Nejat Pishkenari and A. Nemati, Mechanism of C60 rotation and translation on hexagonal boron-nitride monolayer, *J. Chem. Phys.*, 2020, **153**(23), 234702.
40 M. Alves Machado Filho, C.-L. Hsiao, R. B. dos Santos, L. Hultman, J. Birch and G. K. Gueorguiev, Self-Induced Core–Shell InAlN Nanorods: Formation and Stability Unraveled by Ab Initio Simulations, *ACS Nanosci. Au*, 2023, **3**(1), 84–93.
41 D. G. Sangiovanni, R. Faccio, G. K. Gueorguiev and A. Kakanakova-Georgieva, Discovering atomistic pathways for supply of metal atoms from methyl-based precursors to graphene surface, *Phys. Chem. Chem. Phys.*, 2023, **25**(1), 829–837.
42 R. E. Roman and S. W. Cranford, Mechanical properties of silicene, *Comput. Mater. Sci.*, 2014, **82**, 50–55.
43 S. Cahangirov, H. Sahin, G. L. Lay and A. Rubio, *Introduction to the Physics of Silicene and other 2D Materials*. Springer International Publishing, 2016, (Lecture Notes in Physics).
44 M. Ezawa and G. L. Lay, Focus on silicene and other 2D materials, *New J. Phys.*, 2015, **17**(9), 90201.
45 C. Berger, Z. Song, X. Li, X. Wu, N. Brown and C. Naud, *et al.*, Electronic Confinement and Coherence in Patterned Epitaxial Graphene, *Science*, 2006, **312**(5777), 1191–1196.
46 J. C. Meyer, A. K. Geim, M. I. Katsnelson, K. S. Novoselov, T. J. Booth and S. Roth, The structure of suspended graphene sheets, *Nature*, 2007, **446**(7131), 60–63.
47 R. Paul, T. Tasnim, S. Saha and M. Motalab, Atomistic analysis to characterize the impact of temperature and defects on the mechanical properties of germanene sheet, *Mater. Res. Express*, 2018, **5**(1), 15062.
48 H. Oughaddou, H. Enriquez, M. R. Tchalala, H. Yildirim, A. J. Mayne and A. Bendounan, *et al.*, Silicene, a promising new 2D material, *Prog. Surf. Sci.*, 2015, **90**(1), 46–83.
49 H. Zhao, Strain and chirality effects on the mechanical and electronic properties of silicene and silicane under uniaxial tension, *Phys. Lett. A*, 2012, **376**(46), 3546–3550.
50 M. A. Kharadi, G. F. A. Malik, F. A. Khanday, K. A. Shah, S. Mittal and B. K. Kaushik, Review—Silicene: From Material to Device Applications, *ECS J. Solid State Sci. Technol.*, 2020, **9**(11), 115031.
51 M. E. Dávila and G. Le Lay, Silicene: Genesis, remarkable discoveries, and legacy, *Mater. Today Adv.*, 2022, **16**, 100312.
52 M. Z. Hasan and A. H. Romero, Molecular Dynamics Study of Surface Waves on Silicene, *J. Phys. Chem. C*, 2015, **119**(17), 9222–9228.
53 M. Kianezhad, M. Youzi, M. Vaezi and H. Nejat Pishkenari, Rectilinear motion of carbon nanotube on gold surface, *Int. J. Mech. Sci.*, 2022, **217**, 107026.
54 R. Gaisch, R. Berndt, W.-D. Schneider, J. K. Gimzewski, B. Reihl and R. R. Schlittler, *et al.*, Internal structure of C60 on Au(110) as observed by low-temperature scanning tunneling microscopy, *J. Vac. Sci. Technol., B: Microelectron. Nanometer Struct.–Process., Meas., Phenom.*, 1994, **12**(3), 2153–2155.
55 M. T. Cuberes, R. R. Schlittler and J. K. Gimzewski, Room-temperature repositioning of individual C60 molecules at Cu steps: Operation of a molecular counting device, *Appl. Phys. Lett.*, 1996, **69**(20), 3016–3018.
56 Y. Shirai, A. J. Osgood, Y. Zhao, Y. Yao, L. Saudan and H. Yang, *et al.*, Surface-Rolling Molecules, *J. Am. Chem. Soc.*, 2006, **128**(14), 4854–4864.
57 T. Sasaki, J.-F. Morin, M. Lu and J. M. Tour, Synthesis of a single-molecule nanotruck, *Tetrahedron Lett.*, 2007, **48**(33), 5817–5820.
58 S. Kamyabmehr, S. Zoriasatain and L. Farhang Matin, Effects of Stone-Wales defects on optical properties of silicene: DFT study, *Optik (Stuttg)*, 2021, **241**, 166952.
59 R. E. Roman and S. W. Cranford, Defect sensitivity and Weibull strength analysis of monolayer silicene, *Mech. Mater.*, 2019, **133**, 13–25.
60 A. Majumdar, S. Chowdhury, P. Nath and D. Jana, Defect induced magnetism in planar silicene: a first principles study, *RSC Adv.*, 2014, **4**(61), 32221–32227.
61 B. Aufray, A. Kara, S. Vizzini, H. Oughaddou, C. Léandri and B. Ealet, *et al.*, Graphene-like silicon nanoribbons on Ag(110): A possible formation of silicene, *Appl. Phys. Lett.*, 2010, **96**(18), 183102.
62 P. Vogt, P. De Padova, C. Quaresima, J. Avila, E. Frantzeskakis and M. C. Asensio, *et al.*, Silicene: Compelling Experimental Evidence for Graphenelike Two-Dimensional Silicon, *Phys. Rev. Lett.*, 2012, **108**(15), 155501.
63 B. Feng, Z. Ding, S. Meng, Y. Yao, X. He and P. Cheng, *et al.*, Evidence of Silicene in Honeycomb Structures of Silicon on Ag(111), *Nano Lett.*, 2012, **12**(7), 3507–3511.
64 A. Fleurence, R. Friedlein, T. Ozaki, H. Kawai, Y. Wang and Y. Yamada-Takamura, Experimental Evidence for Epitaxial Silicene on Diboride Thin Films, *Phys. Rev. Lett.*, 2012, **108**(24), 245501.
65 M. Rachid Tchalala, H. Enriquez, A. J. Mayne, A. Kara, S. Roth and M. G. Silly, *et al.*, Formation of one-dimensional self-assembled silicon nanoribbons on Au(110)-(2 × 1), *Appl. Phys. Lett.*, 2013, **102**(8), 83107.
66 L. Meng, Y. Wang, L. Zhang, S. Du, R. Wu and L. Li, *et al.*, Buckled Silicene Formation on Ir(111), *Nano Lett.*, 2013, **13**(2), 685–690.

67 J. Feng, Y. Liu, H. Wang, J. Zhao, Q. Cai and X. Wang, Gas adsorption on silicene: A theoretical study, *Comput. Mater. Sci.*, 2014, **87**, 218–226.
68 T. M. Project, Materials Data on Si by Materials Project.
69 V. Bocchetti, H. T. Diep, H. Enriquez, H. Oughaddou and A. Kara, Thermal stability of standalone silicene sheet, *J. Phys.: Conf. Ser.*, 2014, **491**(1), 12008.
70 E. Kolodney, B. Tsipinyuk and A. Budrevich, The thermal stability and fragmentation of C60 molecule up to 2000 K on the milliseconds time scale, *J. Chem. Phys.*, 1994, **100**(11), 8542–8545.
71 M. Eckardt, R. Wieczorek and W. Harneit, Stability of C60 and N@C60 under thermal and optical exposure, *Carbon N Y*, 2015, **95**, 601–607.
72 R. M. Nikonova, V. I. Lad'yanov, S. S. Rekhviashvili and A. V. Pskhu, Thermal Stability of C60 and C70 Fullerites, *High Temp.*, 2021, **59**(2), 179–183.
73 G. R. Berdiyorov and F. M. Peeters, Influence of vacancy defects on the thermal stability of silicene: a reactive molecular dynamics study, *RSC Adv.*, 2014, **4**(3), 1133–1137.
74 P. Erhart and K. Albe, Analytical potential for atomistic simulations of silicon, carbon, and silicon carbide, *Phys. Rev. B: Condens. Matter Mater. Phys.*, 2005, **71**(3), 35211.
75 A. S. M. J. Islam, M. S. Islam, N. Ferdous, J. Park and A. Hashimoto, Vacancy-induced thermal transport in two-dimensional silicon carbide: a reverse non-equilibrium molecular dynamics study, *Phys. Chem. Chem. Phys.*, 2020, **22**(24), 13592–13602.
76 M. H. Rahman, E. H. Chowdhury, M. R. Bin Shahadat and M. M. Islam, Engineered defects to modulate the phonon thermal conductivity of Silicene: A nonequilibrium molecular dynamics study, *Comput. Mater. Sci.*, 2021, **191**, 110338.
77 M.-Q. Le and D.-T. Nguyen, The role of defects in the tensile properties of silicene, *Appl. Phys. A: Mater. Sci. Process.*, 2015, **118**(4), 1437–1445.
78 S. Rouhi, Fracture behavior of hydrogen-functionalized silicene nanosheets by molecular dynamics simulations, *Comput. Mater. Sci.*, 2017, **131**, 275–285.
79 C. Qian and Z. Li, Multilayer silicene: Structure, electronics, and mechanical property, *Comput. Mater. Sci.*, 2020, **172**, 109354.
80 H. Pourmirzaagha and S. Rouhi, Molecular dynamic simulations of the heat transfer in double-layered graphene/silicene nanosheets, *Phys. B*, 2023, **666**, 415079.
81 M. Noshin, A. I. Khan, R. Chakraborty and S. Subrina, Modeling and computation of thermal and optical properties in silicene supported honeycomb bilayer and hetero-bilayer nanostructures, *Mater. Sci. Semicond. Process.*, 2021, **129**, 105776.
82 H.-T. Nguyen, M.-Q. Le and V.-T. Nguyen, Mode-I stress intensity factors of silicene, AlN, and SiC hexagonal sheets, *Mater. Res. Express*, 2018, **5**(6), 65025.
83 M. Khalkhali, A. Rajabpour and F. Khoeini, Thermal transport across grain boundaries in polycrystalline silicene: A multiscale modeling, *Sci. Rep.*, 2019, **9**(1), 5684.
84 Y. Jing, M. Hu and L. Guo, Thermal conductivity of hybrid graphene/silicon heterostructures, *J. Appl. Phys.*, 2013, **114**(15), 153518.
85 M. Hu and D. Poulikakos, Graphene mediated thermal resistance reduction at strongly coupled interfaces, *Int. J. Heat Mass Trans.*, 2013, **62**, 205–213.
86 D. K. Das and J. Sarkar, Comparison of mechanical properties of silicene estimated using different testing procedures: A molecular dynamics study, *J. Appl. Phys.*, 2018, **123**(4), 44304.
87 S. M. Mofidi, H. Nejat Pishkenari, M. R. Ejtehadi and A. V. Akimov, Role of Graphene Surface Ripples and Thermal Vibrations in Molecular Dynamics of C60, *J. Phys. Chem. C*, 2019, **123**(32), 20026–20036.
88 J. Tersoff, Modeling solid-state chemistry: Interatomic potentials for multicomponent systems, *Phys. Rev. B: Condens. Matter Mater. Phys.*, 1989, **39**(8), 5566–5568.
89 N. L. Allinger, Y. H. Yuh and J. H. Lii, Molecular mechanics. The MM3 force field for hydrocarbons. 1, *J. Am. Chem. Soc.*, 1989, **111**(23), 8551–8566.
90 A. K. Rappé and C. J. Casewit, *Molecular Mechanics Across Chemistry*, University Science Books, 1997.
91 N. L. Allinger, Conformational analysis. 130. MM2. A hydrocarbon force field utilizing V1 and V2 torsional terms, *J. Am. Chem. Soc.*, 1977, **99**(25), 8127–8134.
92 E. K. Watkins and W. L. Jorgensen, Perfluoroalkanes: Conformational Analysis and Liquid-State Properties from ab Initio and Monte Carlo Calculations, *J. Phys. Chem. A*, 2001, **105**(16), 4118–4125.
93 P. J. Stephens, F. J. Devlin, C. F. Chabalowski and M. J. Frisch, Ab Initio Calculation of Vibrational Absorption and Circular Dichroism Spectra Using Density Functional Force Fields, *J. Phys. Chem.*, 1994, **98**(45), 11623–11627.
94 K. Kim and K. D. Jordan, Comparison of Density Functional and MP2 Calculations on the Water Monomer and Dimer, *J. Phys. Chem.*, 1994, **98**(40), 10089–10094.
95 C. J. Cramer, *Essentials of Computational Chemistry: Theories and Models*, Wiley, 2005.
96 M. G. Ahangari, M. D. Ganji and A. Jalali, Interaction between fullerene-wheeled nanocar and gold substrate: A DFT study, *Phys E Low-dimensional Syst Nanostructures*, 2016, **83**, 174–179.
97 A. V. Akimov, C. Williams and A. B. Kolomeisky, Charge Transfer and Chemisorption of Fullerene Molecules on Metal Surfaces: Application to Dynamics of Nanocars, *J. Phys. Chem. C*, 2012, **116**(25), 13816–13826.
98 X. Wang, S. Ramírez-Hinestrosa, J. Dobnikar and D. Frenkel, The Lennard-Jones potential: when (not) to use it, *Phys. Chem. Chem. Phys.*, 2020, **22**(19), 10624–10633.
99 F. Shayeganfar and R. Shahsavari, Oxygen- and Lithium-Doped Hybrid Boron-Nitride/Carbon Networks for Hydrogen Storage, *Langmuir*, 2016, **32**(50), 13313–13321.
100 J. H. Lee, A study on a boron-nitride nanotube as a gigahertz oscillator, *J. Korean Phys. Soc.*, 2006, **49**(1), 172–176.

101 S. Plimpton and B. Hendrickson, Parallel Molecular Dynamics Algorithms for Simulation of Molecular Systems, *ACS Publications*, 1995, **592**, 114–132.
102 A. R. Khoei, M. Youzi and G. T. Eshlaghi, Mechanical properties and γ/γ' interfacial misfit network evolution: A study towards the creep behavior of Ni-based single crystal superalloys, *Mech Mater.*, 2022, **171**, 104368.
103 M. Vaezi, H. Nejat Pishkenari and A. Nemati, Mechanism of C60 rotation and translation on hexagonal boron-nitride monolayer, *J. Chem. Phys.*, 2020, **153**(23), 234702.
104 M. Vaezi, H. Nejat Pishkenari and M. R. Ejtehadi, Nanocar swarm movement on graphene surfaces, *Phys. Chem. Chem. Phys.*, 2022, **24**(45), 27759–27771.
105 H. Qian, M. P. Sheetz and E. L. Elson, Single particle tracking. Analysis of diffusion and flow in two-dimensional systems, *Biophys J.*, 1991, **60**(4), 910–921.
106 W. Greiner, L. Neise, H. Stocker, H. Stöcker and D. Rischke, *Thermodynamics and Statistical Mechanics*, Classical theoretical physics, Springer-Verlag, 1995.
107 P. Attard, *Thermodynamics and Statistical Mechanics: Equilibrium by Entropy Maximisation*, Elsevier Science, 2002.
108 D. Ernst and J. Köhler, Measuring a diffusion coefficient by single-particle tracking: Statistical analysis of experimental mean squared displacement curves, *Phys. Chem. Chem. Phys.*, 2013, **15**(3), 845–849.
109 S. Arrhenius, Über die Reaktionsgeschwindigkeit bei der Inversion von Rohrzucker durch Säuren, *Z. Phys. Chem.*, 1889, **4U**, 226–248.
110 S. Chandrasekhar, Stochastic Problems in Physics and Astronomy, *Rev. Mod. Phys.*, 1943, **15**(1), 1–89.
111 J. Gao, J. Zhang, H. Liu, Q. Zhang and J. Zhao, Structures{,} mobilities{,} electronic and magnetic properties of point defects in silicene, *Nanoscale*, 2013, **5**(20), 9785–9792.
112 M. Ozmaian, A. Fathizadeh, M. Jalalvand, M. R. Ejtehadi and S. M. V. Allaei, Diffusion and self-assembly of C60 molecules on monolayer graphyne sheets, *Sci. Rep.*, 2016, **6**(1), 21910.
113 M. Vaezi, H. Nejat Pishkenari and M. R. Ejtehadi, Programmable Transport of C60 by Straining Graphene Substrate, *Langmuir*, 2023, **39**(12), 4483–4494.
114 H. Liu and L. Li, Graphitic materials: Intrinsic hydrophilicity and its implications, *Extrem. Mech. Lett.*, 2017, **14**, 44–50.
115 A. V. Savin and Y. S. Kivshar, Transport of fullerene molecules along graphene nanoribbons, *Sci. Rep.*, 2012, **2**(1), 1012.

